



Preoperative nomogram for predicting spread through air spaces in clinical-stage IA non-small cell lung cancer using ^{18}F -fluorodeoxyglucose positron emission tomography/computed tomography

Yun Wang¹ · Deng Lyu¹ · Chao Cheng² · Taohu Zhou¹ · Wenting Tu¹ · Yi Xiao¹ · Changjing Zuo² · Li Fan¹ · Shiyuan Liu¹

Received: 7 January 2024 / Accepted: 29 February 2024
© The Author(s) 2024

Abstract

Purpose This study aims to assess the predictive value of ^{18}F -fluorodeoxyglucose positron emission tomography/computed tomography (^{18}F -FDG PET/CT) radiological features and the maximum standardized uptake value (SUV_{max}) in determining the presence of spread through air spaces (STAS) in clinical-stage IA non-small cell lung cancer (NSCLC).

Methods A retrospective analysis was conducted on 180 cases of NSCLC with postoperative pathological assessment of STAS status, spanning from September 2019 to September 2023. Of these, 116 cases from hospital one comprised the training set, while 64 cases from hospital two formed the testing set. The clinical information, tumor SUV_{max} , and 13 related CT features were analyzed. Subgroup analysis was carried out based on tumor density type. In the training set, univariable and multivariable logistic regression analyses were employed to identify the most significant variables. A multivariable logistic regression model was constructed and the corresponding nomogram was developed to predict STAS in NSCLC, and its diagnostic efficacy was evaluated in the testing set.

Results SUV_{max} , consolidation-to-tumor ratio (CTR), and lobulation sign emerged as the best combination of variables for predicting STAS in NSCLC. Among these, SUV_{max} and CTR were identified as independent predictors for STAS prediction. The constructed prediction model demonstrated area under the curve (AUC) values of 0.796 and 0.821 in the training and testing sets, respectively. Subgroup analysis revealed a 2.69 times higher STAS-positive rate in solid nodules compared to part-solid nodules. SUV_{max} was an independent predictor for predicting STAS in solid nodular NSCLC, while CTR and an emphysema background were independent predictors for STAS in part-solid nodular NSCLC.

Conclusion Our nomogram based on preoperative ^{18}F -FDG PET/CT radiological features and SUV_{max} effectively predicts STAS status in clinical-stage IA NSCLC. Furthermore, our study highlights that metabolic parameters and CT variables associated with STAS differ between solid and part-solid nodular NSCLC.

Keywords Spread through air spaces · Nomogram · ^{18}F -FDG PET/CT · Non-small cell lung cancer

Yun Wang and Deng Lyu contributed equally to this work.

- ✉ Changjing Zuo
Zuo@qq.com
- ✉ Li Fan
fanli0930@163.com
- ✉ Shiyuan Liu
radiology_cz@163.com

¹ Department of Radiology, Second Affiliated Hospital of Navy Medical University, 415 Fengyang Road, Huangpu District, Shanghai 200003, China

² Department of Nuclear Medicine, Changhai Hospital, Navy Medical University, Shanghai 200433, China

Introduction

According to the 2023 Burden of Cancer Disease Report in China, lung cancer remains one of the malignant tumors with the highest incidence and mortality rates (Qi et al. 2023). In 2015, the World Health Organization (WHO) officially recognized spread through air spaces (STAS) as the fourth invasive pattern of lung adenocarcinoma, in addition to non-lepidic growth, stromal infiltration, vascular and pleural infiltration. STAS is defined as tumor cells extending beyond the tumor edge within the lung parenchyma (Travis et al. 2015; Nicholson et al. 2022), which

can be observed in other type of NSCLC, such as squamous cell carcinoma, lung pleomorphic carcinoma, and lung neuroendocrine tumors (Lu et al. 2017; Yokoyama et al. 2018; Aly et al. 2019). The presence of STAS indicated the presence of potential residual tumor cells in the surgical margins of patients who underwent limited resection such as segmentectomy or wedge resection, resulting in a poorer prognosis (Kadota et al. 2015; Eguchi et al. 2019; Bains et al. 2019; Huang et al. 2022; Ren et al. 2019). More recently, in a meta-analysis to compare prognostic outcomes between lobectomy and sublobar resection in stage I NSCLC patients with STAS, the results indicated that sublobar resection resulted in worse outcomes than lobectomy in stage I NSCLC patients with STAS (Li et al. 2022a, b). Therefore, lobectomy seems to be effective for stage I NSCLC patients with STAS and a comprehensive understanding of STAS is imperative for the judicious selection of suitable surgical modalities.

In fact, a recent report demonstrated negative predictive value of STAS diagnosis on frozen section was extremely low in 48 cases of resected lung adenocarcinoma, even though the diagnostic sensitivity and specificity of STAS on frozen section were 50% and 100% (Walts et al. 2018). It should be noted that there is insufficient published data to support intraoperative detection of STAS.

^{18}F -FDG PET/CT, as a noninvasive imaging method, can simultaneously depict the morphological characteristics and glucose metabolic activity of tumors, exhibiting high accuracy in predicting tumor invasion, lymph node metastasis, and visceral pleural invasion (Volpi et al. 2018; Li et al. 2022a, b; Nakanishii et al. 2021; Wang et al. 2023). Previous studies have indicated correlations between certain CT features of lung cancer and STAS status, offering a potential means of predicting STAS before surgery (Yin et al. 2020). Wang et al. (2020) demonstrated the value of SUV_{max} and total lesion glycolysis (TLG) as indicators for predicting STAS, achieving a diagnostic accuracy of 71.1% and an area under the curve (AUC) value of 0.759. Nishimori et al. (2022) identified an SUV_{max} cut-off value of 2.48, yielding a sensitivity, specificity, and AUC value of 89.5%, 52.8%, and 0.74, respectively. Few studies have explored predicting STAS based on ^{18}F -FDG PET/CT metabolic parameters combined with CT features. The aforementioned studies mainly focused on lung adenocarcinoma, employed variables only based on preoperative ^{18}F -FDG PET/CT metabolic parameters, featured small sample sizes, and lacked external validation.

As far as we know, no previous study on STAS has differentiated between clinical-stage IA NSCLC manifesting as solid or sub-solid nodules at ^{18}F -FDG PET/CT. The SUV_{max} value and CT presentations reflect different levels of histologic aggressiveness within the clinical-stage IA NSCLC spectrum. As a result, it is conceivable that

they also have different incidences and preoperative ^{18}F -FDG PET/CT patterns that affect STAS. Therefore, we sought to analyze the incidence and ^{18}F -FDG PET/CT patterns of STAS in clinical-stage IA NSCLC on the basis of their CT presentation as solid or sub-solid nodules.

This study focused on clinical-stage IA non-small cell lung cancer (NSCLC), excluding pure ground glass nodular (pGGN) lung cancer, which does not exhibit STAS (Kim et al. 2018). Our primary aim was to investigate the risk predictors associated with STAS in this type of lung cancer based on ^{18}F -FDG PET/CT radiological features and SUV_{max} and guide clinical treatment selection and prognosis evaluation while exploring potential differences in the risk variables predicting STAS status in tumors with different densities.

Materials and methods

Patients

Patients diagnosed with clinical-stage IA NSCLC who underwent ^{18}F -FDG PET/CT examination and postoperative pathological evaluation of STAS status were retrospectively analyzed in two hospitals, spanning from September 2019 to September 2023. Clinicopathological data, including gender, age, smoking status, carcinoembryonic antigen levels (CEA), surgical type, lymph node metastasis, and pathological type, were collected for each patient. The inclusion criteria comprised: (1) ^{18}F -FDG PET/CT data obtained within 2 weeks before surgery; (2) clinical-stage IA NSCLC; (3) solid or part-solid nodules in CT presentation; (4) pathological confirmation of NSCLC. Exclusion criteria encompassed: (1) incomplete clinicopathological and radiological data; (2) pGGN; (3) evidence of pathological lymph node or distant metastasis; (4) receipt of preoperative neoadjuvant or chemotherapy; (5) pathological type was not NSCLC. Based on postoperative pathology results, patients were categorized into STAS-positive and STAS-negative groups. The training set comprised 116 cases (45 STAS-positive and 71 STAS-negative) from hospital one, while the testing set included 64 cases (33 STAS-positive and 31 STAS-negative) from hospital two. Figure 1 illustrates the inclusion and exclusion criteria for the cases. In cases where a single patient presents with multiple nodulars meeting the inclusion criteria, we followed the methodology outlined by Derclé et al. (Derclé et al. 2020) to designate a representative nodular with the largest diameter for retrospective analysis.

This study received approval from the Ethics Committee of hospital one (decision number: CZ-20220712-03), and the subjects' informed consent was waived.

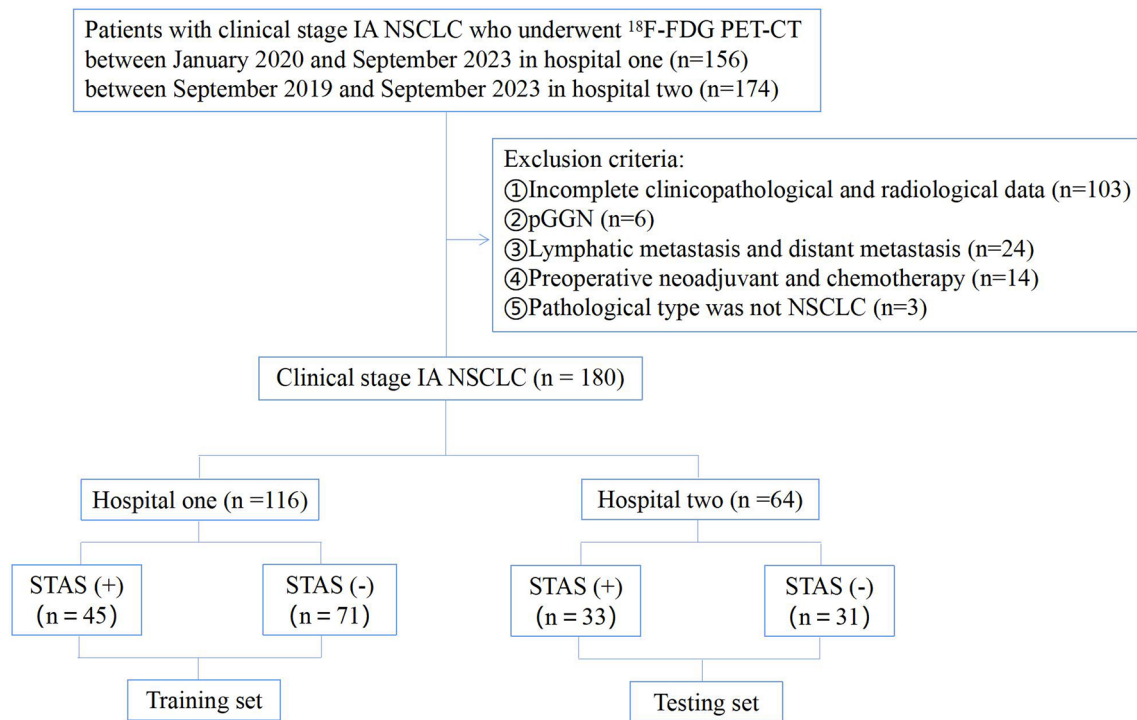


Fig. 1 The flowchart of inclusion and exclusion criteria for the cases

Equipment and parameters

Both the training and testing set underwent whole-body PET/CT tomography utilizing the Siemens Biograph Truepoint64 PET/CT system from Germany. The ^{18}F -FDG used for the scans was supplied by the same company, ensuring a radiochemical purity exceeding 95%. For detailed scanning methods and parameters, refer to Supplemental Content 1.

Image measurement and evaluation

The DICOM images from the patient's ^{18}F -FDG PET/CT scans were imported into Radiant DICOM Viewer software (Version 4.2.1, Medixant, Poland). To display the CT features of the lesions, multi-planar reconstruction (MPR) and maximum intensity projection (MIP) techniques were employed. For quantitative parameter evaluation, two radiologists, each with 7 and 10 years of experience, measured the lesions. The average of their measurements was considered the final result. CT quantitative features included the maximum diameter of the tumor and the maximum diameter of solid components, measured on MPR high-resolution computed tomography (HRCT) lung window images. The consolidation-to-tumor ratio (CTR) was calculated (Suzuki et al. 2011). In terms of measuring metabolic parameters, a region of interest (ROI) covering the tumor was set layer by layer on ^{18}F -FDG PET/CT fusion images, non-tumor areas

were avoided as much as possible. The SUV_{max} value of each slice was automatically generated, and the maximum value from all slices was considered the SUV_{max} value of the tumor. For qualitative features evaluation, two radiologists with 7 and 10 years of experience, respectively, interpreted the CT features of the lesions using a double-blind method. Consensus was reached through consultation in case of differing opinions. HRCT lung window observation included the assessment of tumor density type (solid, part-solid), margin characteristics (lobulation, spiculation), interface definition (well-defined, ill-defined), adjacent features (pleural indentation, vascular convergence, bronchial change), emphysema background, and the presence of Ground glass ribbon sign. Definitions of CT features can be found in Supplemental Table 1.

Pathological diagnosis

The diagnosis of STAS was established using the pathological reports obtained from two hospitals. The diagnostic criteria outlined by the WHO in 2015 were uniformly applied to assess STAS status in both medical facilities (Travis et al. 2015). The evaluation involved the examination of at least two hematoxylin and eosin (HE) stained sections under an optical microscope. Tumor cells in the form of micropapillary clusters, solid nests, or single cells were identified in lung tissues situated more than three alveolar intervals

Table 1 Clinical and pathological datas of patients in the training and testing set

Variables	Training set (<i>n</i> = 116)			Testing set (<i>n</i> = 64)		
	STAS (-) (<i>n</i> = 71)	STAS (+) (<i>n</i> = 45)	<i>P</i> value	STAS (-) (<i>n</i> = 31)	STAS (+) (<i>n</i> = 33)	<i>P</i> value
Gender			0.236 ^a			0.083 ^a
Female	38 (53.5%)	19 (42.2%)		17 (54.8%)	11 (33.3%)	
Male	33 (46.5%)	26 (57.8%)		14 (45.2%)	22 (66.7%)	
Age (year)	64 (58.0,68.0)	65 (57.5,72.0)	0.322 ^c	63.1 ± 8.9	62.6 ± 9.0	0.816 ^d
Smoking status			0.359 ^a			0.196 ^a
Non-smoker	50 (70.4%)	28 (62.2%)		20 (64.5%)	16 (48.5%)	
Smoker	21 (29.6%)	17 (37.8%)		11 (35.5%)	17 (51.5%)	
CEA (µg/L)			0.216 ^a			0.092 ^a
< 5	64 (90.1%)	37 (82.2%)		27 (87.1%)	23 (69.7%)	
≥ 5	7 (9.9%)	8 (17.8%)		4 (12.9%)	10 (30.3%)	
Surgery type			0.407 ^a			1.000 ^b
Sublobectomy	19 (26.8%)	9 (20.0%)		5 (16.1%)	5 (15.2%)	
Lobectomy	52 (73.2%)	36 (80.0%)		26 (83.9%)	28 (84.8%)	
Pathological type			0.037 ^a			0.281 ^a
Adenocarcinoma	66 (93.0%)	36 (80.0%)		26 (83.9%)	24 (72.7%)	
Non-adenocarcinoma	5 (7.0%)	9 (20.0%)		5 (16.1%)	9 (27.3%)	

Note: a, Pearson's Chi-square; b, Yate's correction for continuity; c, the Mann–Whitney U test; d, the two independent samples *t* test; STAS, spread through air spaces; CEA, carcinoembryonic antigen

away from the main tumor boundary. In instances of disagreement, consensus was reached through discussion. The classification of lung cancer adhered to the WHO thoracic tumor classification standard (2021 edition) (Nicholson et al. 2022), and clinical staging was determined according to the Tumor, Node, and Metastasis (TNM) staging criteria (8th edition) for lung cancer (Travis et al. 2016).

Statistical analysis

Statistical analysis was conducted using SPSS 20.0 software and R software (R version 4.2.2). The normality of measurement data was assessed using the Shapiro–Wilk test. Measurement data following a normal distribution were presented as $\bar{x} \pm s$. Group comparisons were made using the independent sample *t* test. Measurement data not conforming to a normal distribution were expressed as M (Q1, Q3), and group comparisons were conducted using the Mann–Whitney U test. Categorical data were presented as the number of cases, and inter-group comparisons were performed using Pearson's Chi-square test, Yate's correction for continuity, or Fisher's exact test. In univariable analysis, a significance level of $P < 0.05$ was considered statistically significant. For the training set, variables with $P < 0.1$ in univariable analysis were included in multivariable logistic regression analysis. Based on the minimization of Akaike information criterion (AIC) (Portet et al. 2020), the optimal combination of predictors was selected to construct the model and the corresponding nomogram was developed. The receiver

operating characteristic (ROC) curve and AUC value were used to evaluate the model's differentiation in the training and external testing set. The DeLong test was used to assess differences in AUC between models. Calibration curves and Hosmer–Lemeshow (H–L) test were used to assess the goodness-of-fit of the model, and the *P* value greater than 0.05 indicated a well goodness-of-fit. Decision curve analysis (DCA) was used to assess the clinical application value of the model. Kappa coefficient and intraclass correlation coefficient (ICC) were utilized to evaluate the consistency of qualitative and quantitative parameters among observers, with $P < 0.05$ considered statistically significant.

Results

Comparison of clinicopathological data

Among the 180 patients diagnosed with NSCLC, 152 cases were identified as LUAD, 24 cases as lung squamous cell carcinoma, 2 cases as lung adenosquamous carcinoma, and 2 cases as large cell lung cancer. In the training set, 45 cases were STAS-positive (38.8%) and 71 cases were STAS-negative (61.2%). In the testing set, 33 cases were STAS-positive (51.6%) and 31 cases were STAS-negative (48.4%). Statistical analysis revealed significant differences in pathological types in the training set ($P < 0.05$) (Table 1). Regarding CT features, the quantitative parameters showed good consistency between the two observers, with ICC values ranging

from 0.960 to 1.000. In addition, the qualitative indicators exhibited strong consistency, with Kappa values ranging from 0.881 to 1.000 (See Supplemental Table 2).

Univariable and multivariable logistic regression analysis

In the training set, the univariable analysis revealed significant differences in SUV_{max}, tumor diameter, solid component diameter, CTR, density type, lobulation, spiculation,

vascular convergence, and Ground glass ribbon sign between the STAS-positive group and the STAS-negative group ($P < 0.05$) (Table 2). Variables with $P < 0.1$ in the univariable analysis were included in the multivariable logistic regression analysis. The results from the multivariable logistic regression analysis identified SUV_{max}, CTR, and lobulation sign as the best predictive variables. SUV_{max} (OR = 1.206) and CTR (OR = 15.92) were identified as independent risk predictors for predicting STAS in NSCLC (Table 3). Subgroup analysis within solid nodular

Table 2 CT features and PET parameters of patients in the training and testing set

Variables	Training set (n = 116)			Testing set (n = 64)		
	STAS (-) (n = 71)	STAS (+) (n = 45)	P value	STAS (-) (n = 31)	STAS (+) (n = 33)	P value
SUV _{max}	1.9 (1.2,4.5)	5.6 (3.8,10.1)	<0.001 ^c	2.9 (1.5,6.8)	10.1 (6.1,13.9)	<0.001 ^c
Tumor diameter	2.1 (1.5,2.6)	2.4 (1.8,2.7)	0.055 ^c	2.1 ± 0.6	2.4 ± 0.4	0.027 ^d
Solid component diameter	1.4 (1.0,1.9)	2.3 (1.7,2.7)	<0.001 ^c	1.6 ± 0.6	2.3 ± 0.5	<0.001 ^d
CTR	0.7 (0.5,1.0)	1.0 (1.0,1.0)	<0.001 ^c	1.0 (0.7,1.0)	1.0 (1.0,1.0)	0.012 ^c
Lymph node uptake			0.143 ^a			0.355 ^b
Absent	56 (78.9%)	30 (66.7%)		28 (90.3%)	26 (78.8%)	
Present	15 (21.1%)	15 (33.3%)		3 (9.7%)	7 (21.2%)	
Density type			<0.001 ^a			0.033 ^a
Part-solid	38 (53.5%)	8 (17.8%)		12 (38.7%)	5 (15.2%)	
Solid	33 (46.5%)	37 (82.2%)		19 (61.3%)	28 (84.8%)	
Interface			0.476 ^a			0.510 ^a
Well-defined	51 (71.8%)	35 (77.8%)		23 (74.2%)	22 (66.7%)	
Ill-defined	20 (28.2%)	10 (22.2%)		8 (25.8%)	11 (33.3%)	
Lobulation			0.012 ^a			0.024 ^b
Absent	20 (28.2%)	4 (8.9%)		8 (25.8%)	1 (3.0%)	
Present	51 (71.8%)	41 (91.1%)		23 (74.2%)	32 (97.0%)	
Spiculation			0.004 ^a			0.313 ^a
Absent	52 (73.2%)	21 (46.7%)		18 (58.1%)	15 (45.5%)	
Present	19 (26.8%)	24 (53.3%)		13 (41.9%)	18 (54.5%)	
Bronchial change			0.916 ^a			0.876 ^a
Absent	23 (32.4%)	15 (33.3%)		9 (29.0%)	9 (27.3%)	
Present	48 (67.6%)	30 (66.7%)		22 (71.0%)	24 (72.7%)	
Pleural indentation			0.224 ^a			0.136 ^a
Absent	35 (49.3%)	17 (37.8%)		14 (45.2%)	9 (27.3%)	
Present	36 (50.7%)	28 (62.2%)		17 (54.8%)	24 (72.7%)	
Vascular convergence			0.004 ^a			0.264 ^a
Absent	52 (73.2%)	21 (46.7%)		22 (71.0%)	19 (57.6%)	
Present	19 (26.8%)	24 (53.3%)		9 (29.0%)	14 (42.4%)	
Emphysema background			0.071 ^a			0.123 ^a
Absent	65 (91.5%)	36 (80.0%)		28 (90.3%)	25 (75.8%)	
Present	6 (8.5%)	9 (20.0%)		3 (9.7%)	8 (24.2%)	
Ground glass ribbon sign			0.031 ^a			0.023 ^a
Absent	46 (64.8%)	20 (44.4%)		21 (67.7%)	13 (39.4%)	
Present	25 (35.2%)	25 (55.6%)		10 (32.3%)	20 (60.6%)	

Note: a, Pearson's Chi-square; b, Yate's correction for continuity; c, the Mann-Whitney U test; d, the two independent samples *t* test; STAS, spread through air spaces; SUV_{max}, the maximum standardized uptake value; CTR, consolidation-to-tumor ratio

Table 3 Univariable and multivariable logistic regression analysis of predictors in the training set

Predictors	Univariable logistic regression analysis		Multivariable logistic regression analysis	
	OR (95% CI)	<i>P</i> value	OR (95% CI)	<i>P</i> value
SUV _{max}	1.308 (1.166–1.497)	<0.001	1.206 (1.067–1.393)	0.005
Tumor diameter	1.905 (1.032–3.638)	0.044		
Solid component diameter	3.571 (2.003–6.780)	<0.001		
CTR	79.49 (10.30–920.5)	<0.001	15.92 (1.516–223.8)	0.027
Density type	5.326(2.262–13.79)	<0.001		
Lobulation	4.020(1.390–14.64)	0.018	3.035(0.926–12.04)	0.083
Spiculation	3.128 (1.437–6.971)	0.005		
Vascular convergence	3.128 (1.437–6.971)	0.005		
Emphysema background	2.708 (0.904–8.662)	0.079		
Ground glass ribbon sign	2.300 (1.078–4.991)	0.033		

Note: OR, odds ratio; CI, confidence interval; SUV_{max}, the maximum standardized uptake value; CTR, consolidation-to-tumor ratio

NSCLC ($n = 70$) showed statistically significant differences in SUV_{max}, tumor diameter, and solid component diameter between the STAS-positive and STAS-negative groups ($P < 0.05$). SUV_{max} (OR = 1.229) was identified as an independent risk predictor for predicting STAS in solid nodular NSCLC. In part-solid nodular NSCLC ($n = 46$), solid component diameter and CTR were significantly different between the STAS-positive and STAS-negative groups ($P < 0.05$). CTR (OR = 7.134) and emphysema background (OR = 2.596) were identified as independent risk predictors for predicting STAS (Table 4). Typical ¹⁸F-FDG PET/CT case images are illustrated in Figs. 2 and 3.

Construction and efficiency analysis of the prediction model

Based on the best combination of the variables identified through multivariable logistic regression analysis, a prediction model was constructed, and a nomogram was

generated (Fig. 4). The regression equation was $\ln(P/1-P) = -4.702 + 2.768 \times \text{CTR} + 0.187 \times \text{SUV}_{\text{max}} + 1.110 \times \text{lobulation}$, where P is the probability of predicting STAS occurrence. The predictive probability value and single predictors of the multivariable logistic regression model were analyzed by the ROC curve. In the training set, the AUC values for CTR, SUV_{max}, and the prediction model in predicting STAS were 0.701, 0.795, and 0.796, with accuracies of 65.52%, 71.55%, and 68.97%, respectively. In the testing set, the AUC values were 0.643, 0.825, and 0.821, respectively, with accuracies of 68.75%, 75.00%, and 78.13% (Table 5). The ROC curve is presented in Fig. 5. The DeLong test indicated that the prediction model was superior to CTR ($Z = 3.181, 3.801, P < 0.05$), and SUV_{max} was better than CTR ($Z = 2.411, 3.105, P < 0.05$). The H-L test demonstrated a good fit for the prediction model in both the training set and the testing set ($P = 0.12, 0.36$) (Fig. 6). DCA illustrated that the prediction model, SUV_{max}, and CTR have good clinical application value (Fig. 7).

Table 4 Univariable and multivariable logistic regression analysis of solid and part-solid nodules in the training set

Predictors	Univariable logistic regression analysis		Multivariable logistic regression analysis	
	OR (95% CI)	<i>P</i> value	OR (95% CI)	<i>P</i> value
Solid nodules				
SUV _{max}	1.229 (1.077–1.445)	0.006	1.229 (1.077–1.445)	0.005
Tumor diameter	2.230 (1.040–5.065)	0.045		
Solid component diameter	2.230 (1.040–5.065)	0.045		
Vascular convergence	2.353 (0.904–6.363)	0.084		
Part-solid nodules				
Solid component diameter	5.255 (0.942–44.05)	0.080		
CTR	12.63 (3.651–205.7)	0.029	7.134 (4.702–9.520)	0.019
Emphysema background	12.33 (1.031–291.6)	0.054	2.596 (1.659–8.121)	0.028

Note: OR, odds ratio; CI, confidence interval; SUV_{max}, the maximum standardized uptake value; CTR, consolidation-to-tumor ratio

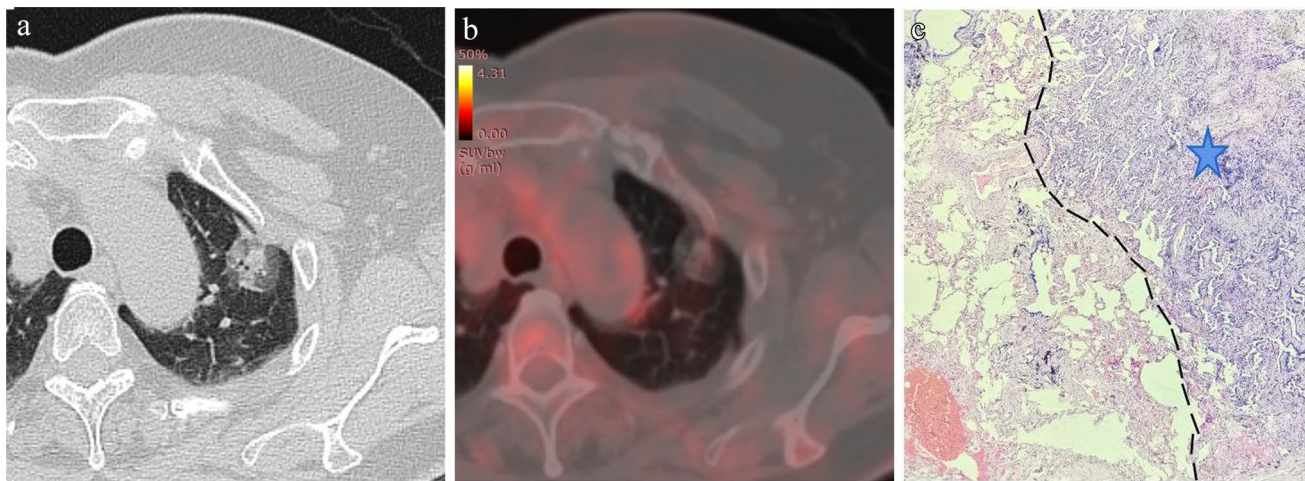


Fig. 2 A 66-year-old female patient with LUAD and negative STAS status. **A** The HRCT shows a part-solid nodule in the left upper lobe of the lung with the longest diameter of the whole tumor and solid component as 2.5 cm and 1.2 cm, respectively. **B** The ^{18}F -FDG PET/

CT shows that the SUV_{max} of the nodule is 0.72. **(C)** Photomicrograph (hematoxylin–eosin stain, magnification 200) shows clean alveolar spaces adjacent to boundary of the tumor (+)

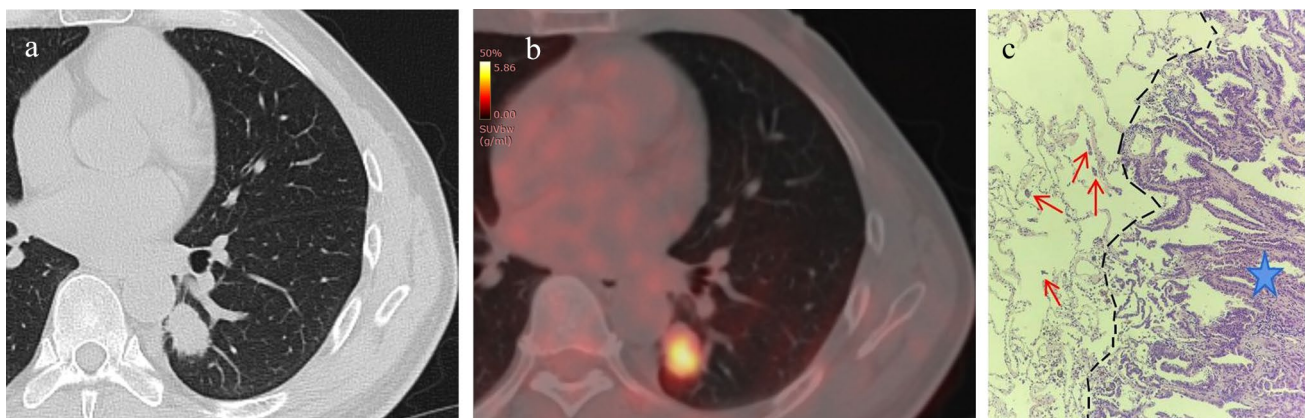


Fig. 3 A 51-year-old male patient with LUAD and positive STAS status. **A** The HRCT shows a solid nodule in the left lower lobe of the lung with the longest diameter of the whole tumor as 2.6 cm. **B** The ^{18}F -FDG PET/CT shows that the SUV_{max} of the nodule is 5.3.

C Photomicrograph (Hematoxylin–eosin stain, magnification 200) shows detached micropapillary clusters of tumor cells (red arrows) in alveolar beyond the edge of the main tumor (+)

Discussion

STAS is a crucial invasive pattern in lung cancer that significantly impacts postoperative tumor recurrence and metastasis. The accurate preoperative assessment of STAS status is essential for effectively stratifying patient risks, guiding surgical method selection, and improving overall survival prognosis. This study identified CTR and SUV_{max} as independent predictors for STAS. The constructed prediction model, incorporating CTR, SUV_{max} , and lobulation, demonstrated excellent diagnostic efficacy with AUC values of 0.796 in the training set and 0.821 in the testing

set. Overall, our nomogram provides a simple and efficient tool for predicting STAS status, offering valuable guidance for clinical treatment decision-making.

In the present study, lobulation, spiculation, vascular convergence, and the Ground glass ribbon sign were more prevalent in the STAS-positive group, aligning with findings in previous literature (Chen et al. 2022; Qi et al. 2021; Toyokawa et al. 2018). Lobulation reflects the expansive growth of the tumor, indicating varying growth rates of cells around the tumor. Spiculation is indicative of tumor tissue invasion into adjacent structures, suggesting increased tumor aggressiveness (Jin et al. 2017). Vascular convergence sign results from tumor infiltration and growth into

Fig. 4 Nomogram for preoperative prediction of STAS status based on ¹⁸F-FDG PET/CT radiological features and SUV_{max} in clinical-stage IA NSCLC

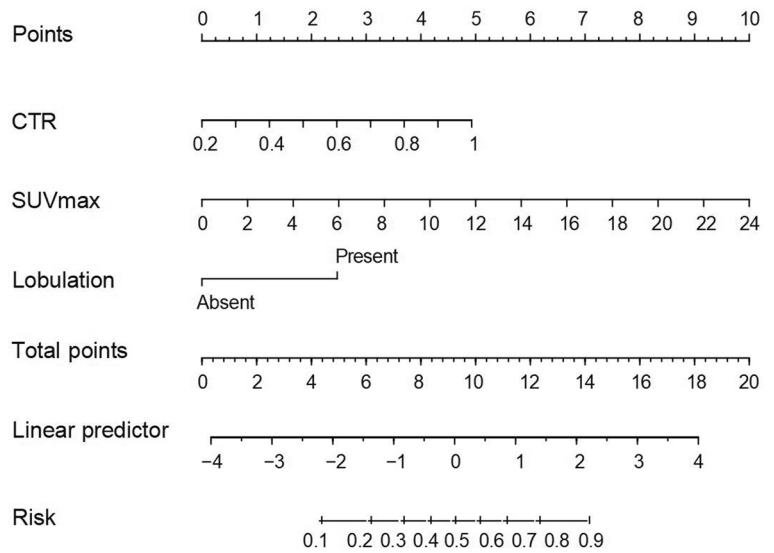


Table 5 The predictive efficacy of CTR, SUV_{max}, and prediction model in the training and testing set

	Set	Cut-off	AUC (95% CI)	Accuracy (%)	Sensitivity (%)	Specificity (%)	PPV (%)	NPV (%)
CTR	Training	0.66	0.701 (0.609–0.783)	65.52%	93.33%	47.89%	53.16%	91.89%
	Testing		0.643 (0.513–0.759)	68.75%	96.97%	38.71%	62.75%	92.31%
SUV _{max}	Training	2.08	0.795 (0.710–0.864)	71.55%	95.56%	56.34%	58.11%	95.24%
	Testing		0.825 (0.709–0.908)	75.00%	72.73%	77.42%	77.42%	72.73%
Prediction model	Training	0.189	0.796 (0.711–0.865)	68.97%	97.78%	50.70%	55.70%	97.30%
	Testing		0.821 (0.705–0.905)	78.13%	84.85%	70.97%	75.68%	81.48%

Note: AUC, area under the curve; CI, confidence interval; PPV, positive predictive value; NPV, negative predictive value; CTR, consolidation-to-tumor ratio; SUV_{max}, the maximum standardized uptake value

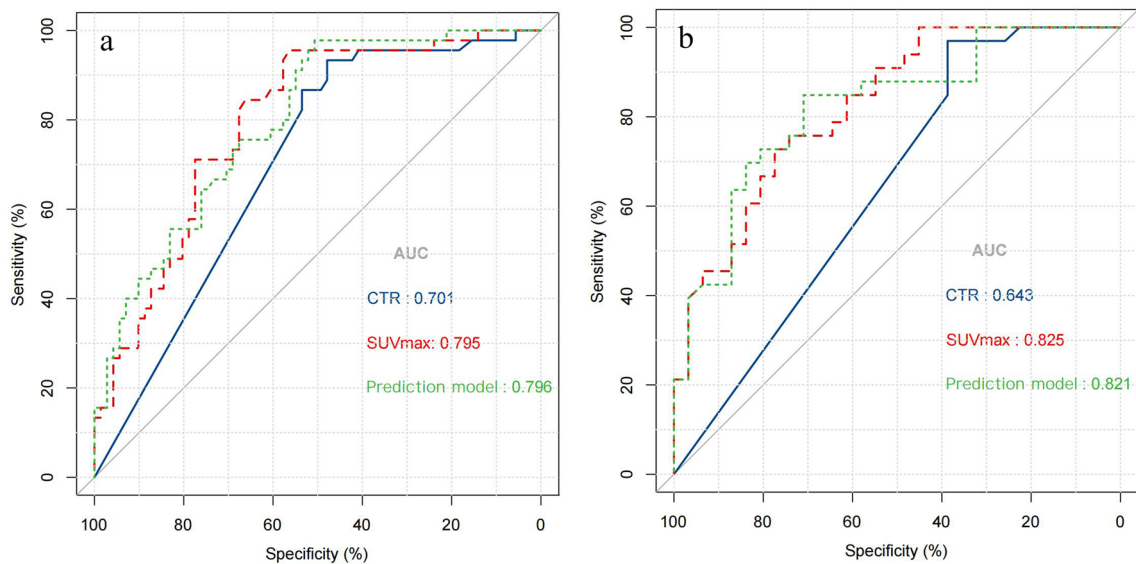


Fig. 5 ROC curve analysis of CTR, SUV_{max}, and the prediction model in the training and testing set

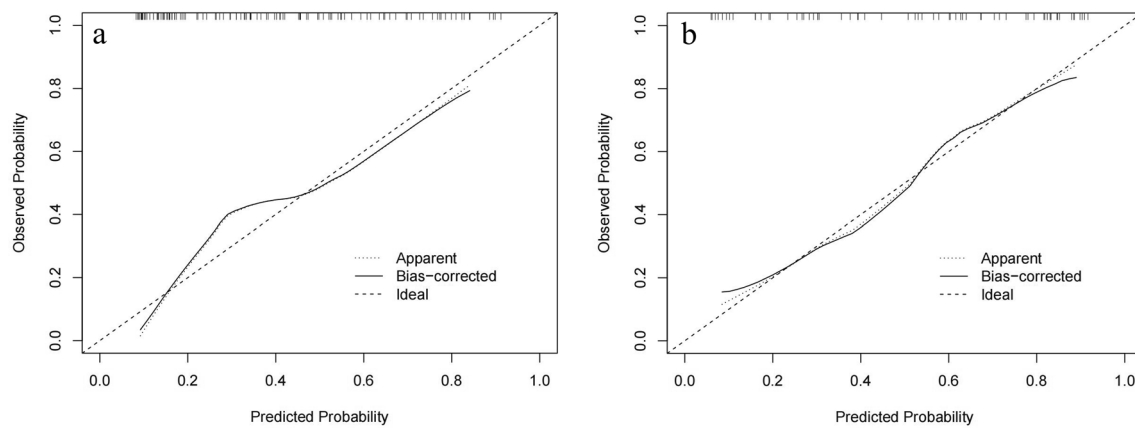


Fig. 6 The calibration curves of the prediction model in the training and testing set

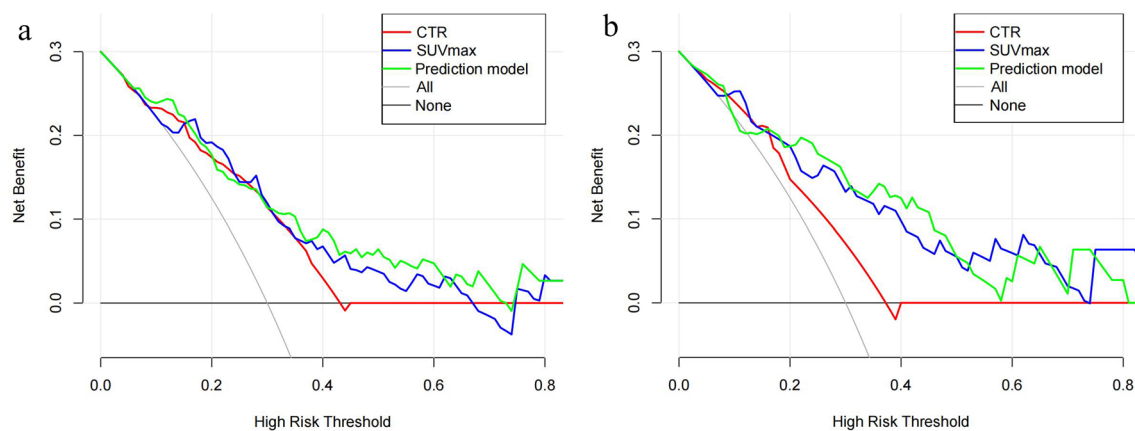


Fig. 7 The decision curves of CTR, SUV_{max} , and the prediction model in the training and testing set

adjacent pulmonary blood vessels and bronchial bundles, with increased fibrous hyperplasia pulling together pulmonary blood vessels (Chen et al. 2022; Zhang et al. 2014), suggesting a greater risk of STAS. The Ground glass ribbon sign, a ribbon shadow extending from the nodule's edge, is speculated to occur when tumor cells escape from the primary lesion, redistribute through the airway, and grow along the surrounding alveolar wall. This leads to the obstruction of surrounding lung parenchyma or bronchioles, resulting in reduced gas content in the alveoli. The presence of the Ground glass ribbon sign was more common in the STAS-positive group, consistent with previous studies (Qi et al. 2021). While the evaluation of CT features is subjective, and previous studies have reached different conclusions, the overall trend suggests that more malignant tumor characteristics increase the likelihood of STAS positivity.

This study observed a positive correlation between tumor diameter, solid component diameter, and CTR with STAS status. The incidence of STAS in solid nodular NSCLC was

2.69 times higher than that in part-solid nodular NSCLC. Multivariable logistic regression analysis confirmed that CTR was an independent risk predictor for predicting STAS, consistent with prior literature reports (Kim et al. 2018; Chen et al. 2022; Qi et al. 2021; Li et al. 2020; Zhang et al. 2020). Compared to tumor diameter and solid component diameter, CTR better represents the more aggressive part of the tumor. The higher the proportion of CTR, the greater the positive rate of STAS, aligning with clinical T staging based on the diameter of the solid component rather than the overall tumor diameter (Travis et al. 2016). Subgroup analysis revealed that CTR and emphysema background were independent risk predictors for predicting STAS in part-solid nodular NSCLC, while SUV_{max} was not a risk predictor for predicting STAS status. It is widely thought that ground glass components in part-solid nodules exhibit slower growth, with fewer tumor cells in this area, resulting in lower maximum FDG uptake than in solid nodules (Travis et al. 2016). This study suggests that CT features

should be emphasized when predicting STAS in part-solid nodular NSCLC.

As the most commonly used semi-quantitative index reflecting the glucose metabolic activity of tumor cells, SUV_{max} can be employed to assess the biological malignancy of tumor cells (de Geus-Oei et al. 2007). In this study, SUV_{max} emerged as an independent risk predictor for predicting STAS. Higher SUV_{max} values indicate stronger metabolic activity and tumor aggressiveness, correlating with an increased positive rate of STAS, consistent with findings from prior studies (Wang et al. 2020; Nishimori et al. 2022). Subgroup analysis revealed that SUV_{max} was an independent risk predictor for predicting STAS in solid nodular NSCLC. These results underscore the importance of careful consideration for the possibility of STAS in clinical-stage IA NSCLC cases with solid nodules on ^{18}F -FDG PET/CT, particularly in instances of elevated SUV_{max} .

This study focused on clinical-stage IA NSCLC, integrating ^{18}F -FDG PET/CT metabolic parameters and CT characteristics associated with STAS. By constructing a nomogram, the intricate regression equation was transformed into a user-friendly graphical tool, aiding in the preoperative assessment of STAS status and assisting in the development of clinical diagnosis plans for patients. In addition, the generalization of the model was further validated using external datasets in this study. The DeLong test demonstrated that the prediction model and SUV_{max} exhibited superior diagnostic efficacy compared to CTR ($P < 0.05$). This suggests that CTR may have certain limitations in predicting STAS, speculating that solid components in tumors may result from fibroblast proliferation, alveolar collapse, inflammatory cell infiltration, and mucous secretion by tumor cells (Park et al. 2007). CTR may not entirely capture the invasiveness of the tumor. On the other hand, SUV_{max} , as an indicator reflecting the FDG metabolism of tumors, represents the proliferative activity of tumor cells and better reflects tumor aggressiveness. In general, a higher SUV_{max} value corresponds to a greater risk of STAS.

This study has several limitations. First, it is a retrospective study, and a certain degree of selection bias is inevitable. Second, the external testing set data in this study are relatively small, and larger multi-center prospective studies are needed to validate the conclusions in the future. Third, with the current focus on radiomics and deep learning, the next steps should involve building a multi-modal deep learning model based on convolutional neural networks, incorporating ^{18}F -FDG PET/CT metabolic parameters, CT features, clinical data, and radiomics features, aiming to assess whether such a model can enhance the diagnostic efficiency of predicting STAS. Fourth, due to the lack of detailed long-term follow-up data, whether STAS is an independent prognostic factor and the effect of STAS on patients undergoing sublobectomy should be further confirmed, we

will conduct this study in the future when more follow-up data are collected.

Conclusion

In conclusion, STAS in clinical-stage IA NSCLC exhibits a strong correlation with ^{18}F -FDG PET/CT parameter information. The nomogram constructed by incorporating SUV_{max} , CTR, and lobulation sign proves to be a valuable tool for predicting STAS status, offering guidance for clinical diagnosis and treatment decisions. Furthermore, SUV_{max} emerges as an independent risk predictor for predicting STAS in solid nodules. For part-solid nodules, prioritizing CTR and assessing emphysema background is recommended. The careful observation of these CT features contributes to enhancing the accuracy of predicting STAS status preoperatively.

Supplementary Information The online version contains supplementary material available at <https://doi.org/10.1007/s00432-024-05674-w>.

Author contributions (I) Conception and design: Dr. Yun Wang and Dr. Deng Lyu. (II) Materials preparation: Dr. Deng Lyu, Dr. Chao Cheng. (III) Collection and analysis of data: Dr. Taohu Zhou and Dr. Wenting Tu. (IV) Manuscript writing: Dr. Yun Wang and Dr. Deng Lyu. (V) Comment on the manuscript: all authors. (VI) Final approval of manuscript: all authors.

Funding This research was funded by National Key R&D Program of China (2022YFC2010000, 2022YFC2010002), Key Program of National Natural Science Foundation of China (81930049), National Natural Science Foundation of China (82171926, 82202140), Shanghai Sailing Program (20YF1449000), Shanghai Science and Technology Innovation Action Plan Program (19411951300), Clinical Innovative Project of Shanghai Changzheng Hospital (2020YLCYJ-Y24), Program of Science and Technology Commission of Shanghai Municipality (21DZ2202600).

Data availability The raw data supporting the conclusions of this article will be made available by the authors, without undue reservation.

Declarations

Ethical approval The authors are accountable for all aspects of the work in ensuring that questions related to the accuracy or integrity of any part of the work are appropriately investigated and resolved. This study was approved by the Ethics Committee of Changzheng Hospital, Naval Medical University (decision number: CZ-20220712-03), and subjects' informed consent was exempted.

Competing interests The authors declare no competing interests.

Open Access This article is licensed under a Creative Commons Attribution 4.0 International License, which permits use, sharing, adaptation, distribution and reproduction in any medium or format, as long as you give appropriate credit to the original author(s) and the source, provide a link to the Creative Commons licence, and indicate if changes were made. The images or other third party material in this article are included in the article's Creative Commons licence, unless indicated otherwise in a credit line to the material. If material is not included in

the article's Creative Commons licence and your intended use is not permitted by statutory regulation or exceeds the permitted use, you will need to obtain permission directly from the copyright holder. To view a copy of this licence, visit <http://creativecommons.org/licenses/by/4.0/>.

References

- Aly RG, Rekhman N, Li X, Takahashi Y, Eguchi T, Tan KS, Rudin CM, Adusumilli PS, Travis WD (2019) Spread through air spaces (STAS) is prognostic in atypical carcinoid, large cell neuroendocrine carcinoma, and small cell carcinoma of the lung. *J Thorac Oncol* 14(9):1583–1593. <https://doi.org/10.1016/j.jtho.2019.05.009>
- Bains S, Eguchi T, Warth A, Yeh YC, Nitadori JI, Woo KM, Chou TY, Dienemann H, Muley T, Nakajima J, Shinozaki-Ushiku A, Wu YC, Lu S, Kadota K, Jones DR, Travis WD, Tan KS, Adusumilli PS (2019) Procedure-specific risk prediction for recurrence in patients undergoing lobectomy or sublobar resection for small (≤ 2 cm) lung adenocarcinoma: an international cohort analysis. *J Thorac Oncol* 14(1):72–86. <https://doi.org/10.1016/j.jtho.2018.09.008>
- Chen Y, Jiang C, Kang W, Gong J, Luo D, You S, Cheng Z, Luo Y, Wu K (2022) Development and validation of a CT-based nomogram to predict spread through air space (STAS) in peripheral stage IA lung adenocarcinoma. *Jpn J Radiol* 40(6):586–594. <https://doi.org/10.1007/s11604-021-01240-3>
- de Geus-Oei LF, van Krieken JH, Aliredjo RP, Krabbe PF, Frielink C, Verhagen AF, Boerman OC, Oyen WJ (2007) Biological correlates of FDG uptake in non-small cell lung cancer. *Lung Cancer* 55(1):79–87. <https://doi.org/10.1016/j.lungcan.2006.08.018>
- Dercle L, Fronheiser M, Lu L, Du S, Hayes W, Leung DK, Roy A, Wilkerson J, Guo P, Fojo AT, Schwartz LH, Zhao B (2020) Identification of non-small cell lung cancer sensitive to systemic cancer therapies using radiomics. *Clin Cancer Res* 26(9):2151–2162. <https://doi.org/10.1158/1078-0432.CCR-19-2942>
- Eguchi T, Kameda K, Lu S, Bott MJ, Tan KS, Montecalvo J, Chang JC, Rekhman N, Jones DR, Travis WD, Adusumilli PS (2019) Lobectomy is associated with better outcomes than sublobar resection in spread through air spaces (STAS)-positive T1 lung adenocarcinoma: a propensity score-matched analysis. *J Thorac Oncol* 14(1):87–98. <https://doi.org/10.1016/j.jtho.2018.09.005>
- Huang L, Tang L, Dai L, Shi Y (2022) The prognostic significance of tumor spread through air space in stage I lung adenocarcinoma. *Thorac Cancer* 13(7):997–1005. <https://doi.org/10.1111/1759-7714.14348>
- Jin C, Cao J, Cai Y, Wang L, Liu K, Shen W, Hu J (2017) A nomogram for predicting the risk of invasive pulmonary adenocarcinoma for patients with solitary peripheral subsolid nodules. *J Thorac Cardiovasc Surg* 153(2):462–469.e1. <https://doi.org/10.1016/j.jtcvs.2016.10.019>
- Kadota K, Nitadori JI, Sima CS, Ujiie H, Rizk NP, Jones DR, Adusumilli PS, Travis WD (2015) Tumor spread through air spaces is an important pattern of invasion and impacts the frequency and location of recurrences after limited resection for small stage I lung adenocarcinomas. *J Thorac Oncol* 10(5):806–814. <https://doi.org/10.1097/JTO.0000000000000486>
- Kim SK, Kim TJ, Chung MJ, Kim TS, Lee KS, Zo JI, Shim YM (2018) Lung adenocarcinoma: CT features associated with spread through air spaces. *Radiology* 289(3):831–840. <https://doi.org/10.1148/radiol.2018180431>
- Li C, Jiang C, Gong J, Wu X, Luo Y, Sun G (2020) A CT-based logistic regression model to predict spread through air space in lung adenocarcinoma. *Quant Imaging Med Surg* 10(10):1984–1993. <https://doi.org/10.21037/qims-20-724>
- Li J, Wang Y, Li J, Cao S, Che G (2022a) Meta-analysis of lobectomy and sublobar resection for stage I non-small cell lung cancer with spread through air spaces. *Clin Lung Cancer* 23(3):208–213. <https://doi.org/10.1016/j.clcl.2021.10.004>
- Li XF, Shi YM, Niu R, Shao XN, Wang JF, Shao XL, Zhang FF, Wang YT (2022b) Risk analysis in peripheral clinical T1 non-small cell lung cancer correlations between tumor-to-blood standardized uptake ratio on 18F-FDG PET-CT and primary tumor pathological invasiveness: a real-world observational study. *Quant Imaging Med Surg* 12(1):159–171. <https://doi.org/10.21037/qims-21-394>
- Lu S, Tan KS, Kadota K, Eguchi T, Bains S, Rekhman N, Adusumilli PS, Travis WD (2017) Spread through air spaces (STAS) Is an independent predictor of recurrence and lung cancer-specific death in squamous cell carcinoma. *J Thorac Oncol* 12(2):223–234. <https://doi.org/10.1016/j.jtho.2016.09.129>
- Nakanishi K, Nakamura S, Sugiyama T, Kadomatsu Y, Ueno H, Goto M, Ozeki N, Fukui T, Iwano S, Chen-Yoshikawa TF (2021) Diagnostic utility of metabolic parameters on FDG PET/CT for lymph node metastasis in patients with cN2 non-small cell lung cancer. *BMC Cancer* 21(1):983. <https://doi.org/10.1186/s12885-021-08688-6>
- Nicholson AG, Tsao MS, Beasley MB, Borczuk AC, Brambilla E, Cooper WA, Dacic S, Jain D, Kerr KM, Lantuejoul S, Noguchi M, Papotti M, Rekhman N, Scagliotti G, van Schil P, Sholl L, Yatabe Y, Yoshida A, Travis WD (2022) The 2021 WHO classification of lung tumors: impact of advances since 2015. *J Thorac Oncol* 17(3):362–387. <https://doi.org/10.1016/j.jtho.2021.11.003>
- Nishimori M, Iwasa H, Miyatake K, Nitta N, Nakaji K, Matsumoto T, Yamanishi T, Yoshimatsu R, Iguchi M, Tamura M, Yamagami T (2022) ^{18}F FDG-PET/CT analysis of spread through air spaces (STAS) in clinical stage I lung adenocarcinoma. *Ann Nucl Med* 36(10):897–903. <https://doi.org/10.1007/s12149-022-01773-1>
- Park CM, Goo JM, Lee HJ, Lee CH, Chun EJ, Im JG (2007) Nodular ground-glass opacity at thin-section CT: histologic correlation and evaluation of change at follow-up. *Radiographics* 27(2):391–408. <https://doi.org/10.1148/rg.272065061>
- Portet S (2020) A primer on model selection using the Akaike Information Criterion. *Infect Dis Model* 5:111–128. <https://doi.org/10.1016/j.idm.2019.12.010>
- Qi L, Xue K, Cai Y, Lu J, Li X, Li M (2021) Predictors of CT morphologic features to identify spread through air spaces preoperatively in small-sized lung adenocarcinoma. *Front Oncol* 10:548430. <https://doi.org/10.3389/fonc.2020.548430>
- Qi J, Li M, Wang L, Hu Y, Liu W, Long Z, Zhou Z, Yin P, Zhou M (2023) National and subnational trends in cancer burden in China, 2005–20: an analysis of national mortality surveillance data. *Lancet Public Health* 8(12):e943–e955. [https://doi.org/10.1016/S2468-2667\(23\)00211-6](https://doi.org/10.1016/S2468-2667(23)00211-6)
- Ren Y, Xie H, Dai C, She Y, Su H, Xie D, Zheng H, Zhang L, Jiang G, Wu C, Chen C (2019) Prognostic impact of tumor spread through air spaces in sublobar resection for IA lung adenocarcinoma patients. *Ann Surg Oncol* 26(6):1901–1908. <https://doi.org/10.1245/s10434-019-07296-w>
- Suzuki K, Koike T, Asakawa T, Kusumoto M, Asamura H, Nagai K, Tada H, Mitsudomi T, Tsuboi M, Shibata T, Fukuda H, Kato H, Japan Lung Cancer Surgical Study Group (JCOG LCSSG) (2011) A prospective radiological study of thin-section computed tomography to predict pathological noninvasiveness in peripheral clinical IA lung cancer (Japan Clinical Oncology Group 0201). *J Thorac Oncol* 6(4):751–756. <https://doi.org/10.1097/JTO.0b013e31821038ab>
- Toyokawa G, Yamada Y, Tagawa T, Kamitani T, Yamasaki Y, Shimokawa M, Oda Y, Maehara Y (2018) Computed tomography features of resected lung adenocarcinomas with spread through air spaces. *J Thorac Cardiovasc Surg* 156(4):1670–1676.e4. <https://doi.org/10.1016/j.jtcvs.2018.04.126>

- Travis WD, Brambilla E, Nicholson AG, Yatabe Y, Austin JHM, Beasley MB, Chirieac LR, Dacic S, Duhig E, Flieder DB, Geisinger K, Hirsch FR, Ishikawa Y, Kerr KM, Noguchi M, Pelosi G, Powell CA, Tsao MS, Wistuba I, WHO Panel (2015) The 2015 world health organization classification of lung tumors: impact of genetic, clinical and radiologic advances since the 2004 classification. *J Thorac Oncol* 10(9):1243–1260. <https://doi.org/10.1097/JTO.0000000000000630>
- Travis WD, Asamura H, Bankier AA, Beasley MB, Detterbeck F, Flieder DB, Goo JM, MacMahon H, Naidich D, Nicholson AG, Powell CA, Prokop M, Rami-Porta R, Rusch V, van Schil P, Yatabe Y, International Association for the Study of Lung Cancer Staging and Prognostic Factors Committee and Advisory Board Members (2016) The IASLC lung cancer staging project: proposals for coding T categories for subsolid nodules and assessment of tumor size in part-solid tumors in the forthcoming eighth edition of the TNM classification of lung cancer. *J Thorac Oncol* 11(8):1204–1223. <https://doi.org/10.1016/j.jtho.2016.03.025>
- Volpi S, Ali JM, Tasker A, Peryt A, Aresu G, Coonar AS (2018) The role of positron emission tomography in the diagnosis, staging and response assessment of non-small cell lung cancer. *Ann Transl Med* 6(5):95. <https://doi.org/10.21037/atm.2018.01.25>
- Walts AE, Marchevsky AM (2018) Current evidence does not warrant frozen section evaluation for the presence of tumor spread through alveolar spaces. *Arch Pathol Lab Med* 142(1):59–63. <https://doi.org/10.5858/arpa.2016-0635-OA>
- Wang XY, Zhao YF, Yang L, Liu Y, Yang YK, Wu N (2020) Correlation analysis between metabolic tumor burden measured by positron emission tomography/computed tomography and the 2015 World Health Organization classification of lung adenocarcinoma, with a risk prediction model of tumor spread through air spaces. *Transl Cancer Res* 9(10):6412–6422. <https://doi.org/10.21037/tcr-20-1934>
- Wang Y, Lyu D, Zhou T, Tu W, Fan L, Liu S (2023) Multivariate analysis based on the maximum standard unit value of 18F-fluorodeoxyglucose positron emission tomography/computed tomography and computed tomography features for preoperative predicting of visceral pleural invasion in patients with subpleural clinical stage IA peripheral lung adenocarcinoma. *Diagn Interv Radiol* 29(2):379–389. <https://doi.org/10.4274/dir.2023.222006>
- Yin Q, Wang H, Cui H, Wang W, Yang G, Qie P, Xun X, Han S, Liu H (2020) Meta-analysis of association between CT-based features and tumor spread through air spaces in lung adenocarcinoma. *J Cardiothorac Surg* 15(1):243. <https://doi.org/10.1186/s13019-020-01287-9>
- Yokoyama S, Murakami T, Tao H, Onoda H, Hara A, Miyazaki R, Furukawa M, Hayashi M, Inokawa H, Okabe K, Akagi Y (2018) Tumor spread through air spaces identifies a distinct subgroup with poor prognosis in surgically resected lung pleomorphic carcinoma. *Chest* 154(4):838–847. <https://doi.org/10.1016/j.chest.2018.06.007>
- Zhang Y, Qiang JW, Ye JD, Ye XD, Zhang J (2014) High resolution CT in differentiating minimally invasive component in early lung adenocarcinoma. *Lung Cancer* 84(3):236–241. <https://doi.org/10.1016/j.lungcan.2014.02.008>
- Zhang Z, Liu Z, Feng H, Xiao F, Shao W, Liang C, Sun H, Gu X, Liu D (2020) Predictive value of radiological features on spread through air space in stage cIA lung adenocarcinoma. *J Thorac Dis* 12(11):6494–6504. <https://doi.org/10.21037/jtd-20-1820>

Publisher's Note Springer Nature remains neutral with regard to jurisdictional claims in published maps and institutional affiliations.